Results in Physics 19 (2020) 103373

Contents lists available at ScienceDirect

Results in Physics

journal homepage: www.elsevier.com/locate/rinp

Tunable violet radiation in a quasi-phase-matched periodically poled stoichiometric lithium tantalate waveguide by direct femtosecond laser writing

LingQi Li[a], Bin Zhang[a], Carolina Romero[b], Javier R. Vázquez de Aldana[b], Lei Wang[a,c,*], Feng Chen[a]

[a] School of Physics, State Key Laboratory of Crystal Materials, Shandong University, Jinan 250100, China
[b] Grupo de Investigación en Aplicaciones del Láser y Fotónica, Departamento de Física Aplicada, University of Salamanca, Salamanca 37008, Spain
[c] Collaborative Innovation Center of Light Manipulations and Applications, Shandong Normal University, Jinan 250358, China

ARTICLE INFO

Keywords:
Violet light
Waveguide
Femtosecond laser writing
Quasi phase matching
Periodically poled stoichiometric lithium tantalate

ABSTRACT

We report on violet-light generation using the femtosecond-laser written waveguides in periodically poled MgO:$LiTaO_3$ crystal under conditions of third-order quasi-phase matching. Ten parallel depressed cladding waveguides are successfully fabricated with different grating periods in the same sample with fan-out $\chi^{(2)}$ grating structures. These waveguides exhibit high optical quality with minimum insertion loss as low as 0.71 dB. Temperature and wavelength tuned second harmonic generation for different waveguides are demonstrated by using a tunable CW Ti sappire laser. Tunable violet second harmonic light has been generated with a single period over the range of 396 nm to 401 nm by varying the crystal temperature from 60 °C to 200 °C. At the quasi-phase matching temperature, 0.37 mW of violet light power at 397.2 nm is generated for a fundamental power of 336.7 mW, corresponding to a normalized conversion efficiency of 0.39%/(W·cm^2). Our work contributes to designing tunable and efficient on-chip violet light sources based on femtosecond-laser written waveguides.

Introduction

Compact and stable violet laser sources have attracted much attention due to their various applications including optical communication [1], ultrafast spectroscopy [2], high-density optical data storage [3] and quantum optics [4]. In recent research, especially, a 397 nm ultraviolet laser is in great demand to generate polarization squeezed and entangled states in the field of quantum information networks [5]. Second harmonic generation (SHG) of near-infrared laser by means of quasi-phase matched (QPM) is one of the most prominent approaches to access efficient violet spectral radiation because it has significant advantages in accessing the higher nonlinear coefficients d_{33} and permitting phase matching at any wavelength within the transparency range of the nonlinear crystal by using an dispersion determined domain-inverted period [6–9]. In general, the domain-inverted grating is fixed at a single period, restricting some tunable wavelength applications over a broad spectral range. Therefore, the design of fan-structured domain-inverted grating pattern is desired for permitting seamlessly varying poling period [10–12]. Recently, periodically poled ferroelectrics, e.g., periodically poled $LiNbO_3$ (PPLN), $KTiOPO_4$ (PPKTP) and $LiTaO_3$ (PPLT) have been widely exploited for QPM interactions. However the violet spectral region is at the transmission cut-off wavelength of LN and poling LN so that SHG in the violet spectral range requires a lifted temperature [13]. Besides, PPKTP is suffering severe absorption and disadvantage of grey tracking effect in violet spectral range [14]. In contrast, periodically poled MgO doped stoichiometric lithium tantalate (PPMgSLT) crystal is an attractive choice for violet SHG owing to its broad transparency range (0.28–5.5 μm), relatively high effective nonlinear coefficient ($d_{33} \approx 13$ pm/V) and high optical damage threshold.[15–17] Nevertheless, violet light generation using the QPM approach has been challenging, due to the facts that the dispersion increases rapidly at the violet wavelength. The short $\chi^{(2)}$ grating for the 1st QPM is also difficult to fabricated over a long interaction length for thick crystals [18,19]. To overcome this limitations, high-order QPM interaction and Type-II QPM SHG are proposed to obtain the violet-wavelength output which require the longer domain-inverted grating period. An apparent drawback of Type-II QPM is that one can't employ the highest nonlinear coefficient d_{33}, instead, using a smaller nonlinear component d_{24} in KTP [20]. The higher-order QPM SHG could be employed to increase the

* Corresponding author.
E-mail address: leiwangsdu@sdu.edu.cn (L. Wang).

https://doi.org/10.1016/j.rinp.2020.103373
Received 4 May 2020; Received in revised form 26 August 2020; Accepted 28 August 2020
Available online 02 September 2020

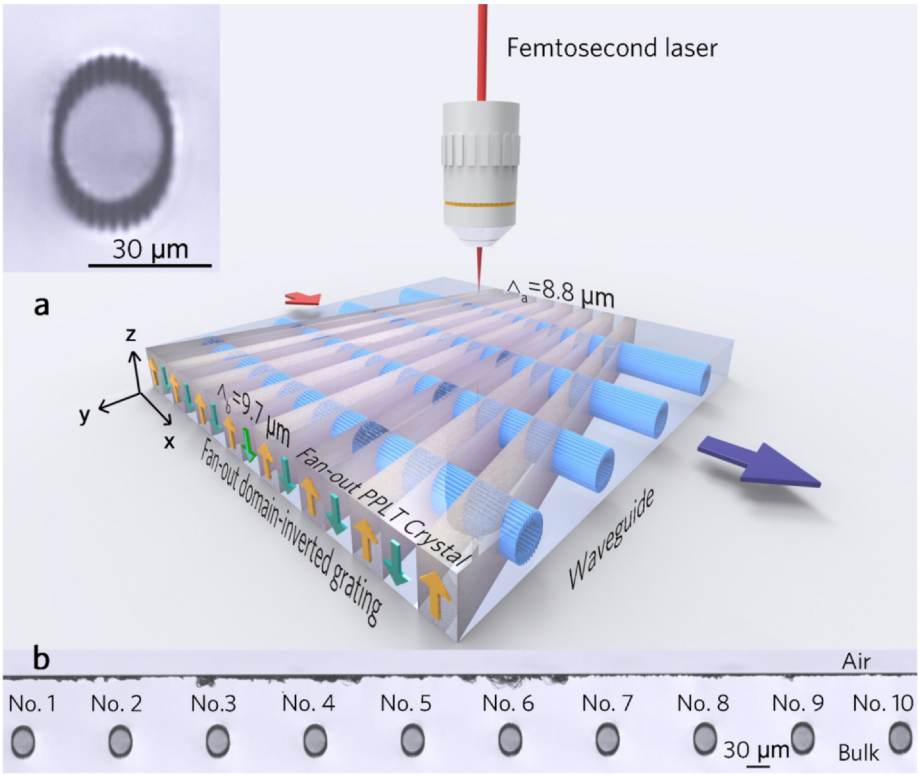

Fig. 1. The fabrication of cladding waveguides by femtosecond laser direct writing in fan-out PPMgSLT crystal. (a) The schematic plot of the a waveguide-type QPM SHG device based on a fan-out domain-inverted structure with grating period seamlessly vary from 8.8 to 9.7 μm. Inset picture is a larger microscope image of the circular waveguides with diameter of 30 μm. (b) Optical microscope cross-sectional image of waveguides No. 1 to No. 10 separated by 100 μm, corresponding to 8.82 to 9.00 μm.

grating period, making it easier to realize homogeneous poling throughout large crystal volume, but at the expense of the limited conversion efficiency and a resulted small d_{eff} [21,22].

Optical waveguides confine the light in the manner of waveguide modes with micrometric or sub-micrometric scales, which can eliminate the diffraction and walk-off effect during the light propagation. Higher optical intra-cavity intensities could be generated compared to the bulk setup of the same materials [23]. Thereby, a QPM-SHG device based on waveguide structure is preferred for realization higher conversion efficiency as a result of a long interaction length and a large spatial mode overlapping at the higher light intensity [24–26]. Optical waveguide in LT crystal is normally fabricated by annealed proton exchange, suffering the disadvantages of geometry close to surface and degraded nonlinear properties [27,28]. Most recently, femtosecond laser direct writing has become a powerful and unique technique to fabricate three-dimensional guiding structures in various crystals, showing the superiority of flexible patterning, negligible effect of thermal-diffusion, and capability for maskless 3D processing [29–33]. Tight focused femtosecond laser pulses could modify the optical properties in the focal volume though nonlinear processes such as tuning ionization, multiphoton absorption and avalanche ionization. Hence, permanent and stable refractive-index modification may be created, which could be used for waveguide fabrication [34–36]. This technique has the potential to fabricate high quality waveguides to realize efficient SHG. Particularly, the geometry of cladding waveguides is more favorable due to the undamaged circular waveguide core surrounded by many low-index laser-written tracks, permitting access to efficient frequency conversion by preserving the large nonlinear coefficient of bulk [37–39]. Up to now, several groups have demonstrated femtosecond laser-written waveguides for efficient frequency doubling in LN [40], PPLN [41], KTP [42], PPKTP [43] and BiB_3O_6 (BIBO) [44] crystals in different waveguide configurations, including our previous work about the efficient QPM SHG in PPLT crystal. However, these work mainly focus on the SHG at the blue and green spectral region. In the violet spectral radiation, Y. Jia *et al* have reported the SHG of violet light in femtosecond-laser-inscribed BIBO cladding waveguides using the birefringent phase matching [45]. S. Campbell *et al* have investigated the violet light generation using a femtosecond laser-written Type I waveguides in PPKTP crystal under the condition of third-order QPM [46]. Nevertheless, the SHG conversion efficiency of this work is limited to $0.02\%W^{-1}$ due to the waveguide region disrupt the periodically-inverted domain structure and the high propagation loss. In addition, in organic crystal, Almeida *et al* have reported SHG at 377 nm in femtosecond laser inscribed cladding waveguide, which supports multimode guidance [47]. A high quality waveguide preserved the nonlinear properties of original bulk material is still absent. And there has been no investigation of the violet light generation in femtosecond laser-written waveguides in PPLT crystal.

In this work, we demonstrate the violet light generation in the cladding waveguides fabricated by femtosecond laser direct writing in PPMgSLT crystal. Ten depressed cladding waveguides separated by 100 μm with high optical quality are inscribed at the fan-out sample, corresponding to different grating periods which satisfied the 3rd QPM. We investigate the wavelength dependence of the critical phase matched temperature at each waveguides. The violet laser is tunable from 394.5 nm to 404.5 nm by varying the crystal temperature from 60 °C to 200 °C. A comparable normalized conversion efficiency of 0.39%/($W{\cdot}cm^2$) is obtained for 8.94 μm period.

Experiments in details

The *z*-cut fan-out MgO (1 mol%) doped PPSLT crystal used in this work is cut into the dimensions of 0.5 (*z*) × 11 (*x*) × 7 (*y*) mm^3. A fan out $\chi^{(2)}$ grating structure is across the width of the crystal with spatially varying grating period from 8.8 μm to 9.7 μm. To fabricate cladding waveguides, an amplified Ti:Sapphire laser system (Spitfire, Spectra Physics) is used as the laser source, generating linear polarized laser pulses at a central wavelength of 800 nm with temporal duration of 120 fs (1 kHz repetition rate/1 mJ maximum pulse energy). A calibrated neutral density filter and a half-wave plate is used to control the irradiate pulse energy. The sample is placed in a PC-controlled 3D motorized stage with a spatial resolution of 100 nm. Several tests at

different pulse energies and scanning speed is performed to find the optimum fabrication parameters. The final irradiation condition is a pulse energy of 0.22 μJ with a scanning speed of 500 μm/s to avoid the formation of multi-foci which is induced by self-focusing of the light, thus create a onefold track with large enough refractive-index modification. Fig. 1(a) shows the schematic illustration of waveguide fabrication process by femtosecond laser. During the writing process, the laser beam is focus below the sample surface (11 × 7 mm^2) utilizing 40× microscope objective (N.A. = 0.65). The sample is moving along the *x*-axis, forming the desired damage track. 28 parallel elliptical tracks at different depths of the sample are performed to inscribe the circular cladding waveguide structure with a diameter of 30 μm. Ten individual waveguides are successfully fabricated in the same substrate separated by 100 μm.

After the femtosecond laser writing, the two end-faces of the crystal is polished for characterizing the propagation properties of the waveguides. The cross-sectional microscope images of the cladding waveguides is taken by using an optical microscope (Axio Imager, Carl Zeiss) operating in transmission mode. A typical end-face coupling system is arranged to collect the near-field mode profiles. The insertion loss is estimated by direct measuring the input power and output power of the transmitted laser beam.

To experimentally generate the SH light from QPM, a continuous-wave (CW) tunable Ti:Sapphire laser (Coherent MBR 110) is employed as the fundamental frequency light source. The schematic of the experiment set up is depicted in Fig. 2(a). A half-wave plate is inserted to calibrate the laser polarization along TM polarization to realize maximum nonlinear coefficient, d_{33}. The polarized laser beam is coupled into the waveguide by convex lens with focal length of f = 25 mm. The frequency doubling light emitted from the output end face is captured by a microscope objective lens (N.A. = 0.4). Afterwards, the generated SH light is separated from fundamental frequency light by using an optical low pass filter (OLPF). The model profile and power of the output light are monitored with a CCD camera and a power meter. The emission spectra of waveguide laser was analyzed by a calibrated spectrometer (Zolix, SGM100 Spectrograph) with resolution of 0.01 nm. During the characterization, the sample is placed inside oven (Thorlabs, PV10) to realize the temperature tuning QPM, in which the operation temperature can be varied up to 200 °C with an accuracy of 0.1 °C.

Theory and waveguide properties

As schematically shown in Fig. 1(a). These waveguides separated by 100 μm situate perpendicularly along the periodically poled structure at different position. Fig. 1(b) shows the optical transmission microscopy image of the cross section of the PPMgSLT cladding waveguides Nos. 1–10, corresponding to the different periods of 8.82, 8.84, 8.86, 8.88, 8.90, 8.92, 8.94, 8.96, 8.98, 9.00 μm with a step of 0.02 μm, respectively. As shown in the inset image of Fig. 1(a), the waveguide exhibits a nearly perfect circular geometry with 28 elliptical laser-written tracks. All the waveguides process the same diameter of 30 μm under the same fabrication process, implying our methods have the efficient reproducibility. The insertion loss of ten waveguides are performed at 1064 nm by taking the Fresnel reflection loss into account, which is present in Table 1. Apparently, all the insertion loss are less than 1.5 dB, including the propagation loss and the coupling loss between the launched focus spot and the waveguide mode profile.

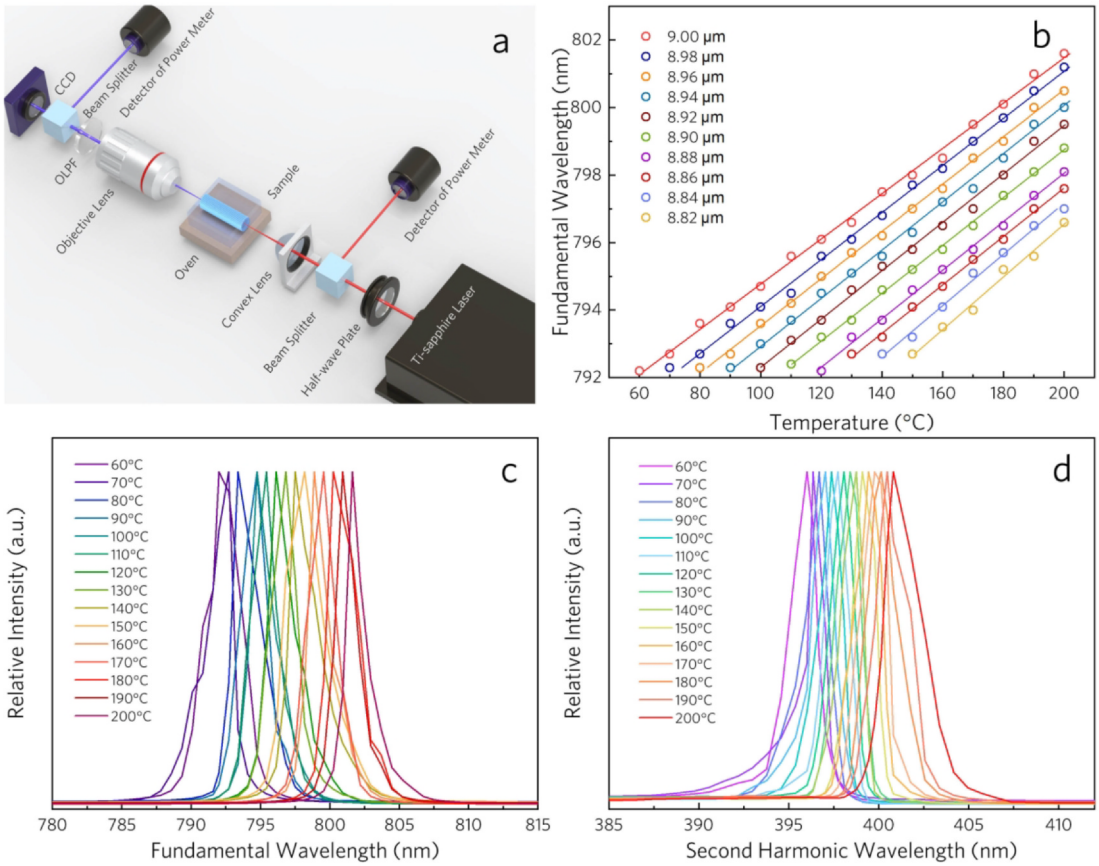

Fig. 2. (a) Schematic diagram of experimental set up for SHG cladding waveguides using a cw tunable Ti:sapphire laser. (b) Experimental phase-matched fundamental wavelength as a function of the PPMgLT crystal temperature for ten waveguides with different grating periods ranging from 8.82 to 9.00 μm, in increments of 0.02 μm. (c) Series of spectral profile for the fundamental wavelength at different crystal temperature at waveguide No. 10 (grating period of 9.00 μm). (d) Corresponding series of the SH wavelength measured at their QPM wavelength of different temperature.

Table 1
The waveguides properties for QPM SHG in violet range.

Waveguides	Poling period (μm)	Insertion loss at 1064 nm (dB)		SH properties at 794.4 nm input	
		TE	TM	Maximum SH power (mW)	Norm. efficiency %/(W·cm^2)
No.1	8.82	1.12	1.32	0.21	0.23
No.2	8.84	0.83	1.25	0.24	0.32
Mo.3	8.86	0.72	0.93	0.32	0.36
No.4	8.88	0.93	1.43	0.20	0.22
No.5	8.90	1.16	1.21	0.23	0.31
No.6	8.92	0.79	0.82	0.35	0.38
No.7	8.94	1.03	1.27	0.22	0.26
No.8	8.96	0.74	0.79	0.37	0.39
No.9	8.98	0.84	1.04	0.27	0.32
N0.10	9.00	0.71	1.17	0.22	0.31

The grating period required for first-order QPM condition is ~2.87 μm at 60 °C around 795 nm in PPLT crystal. At present, such a small period is quiet difficult to achieve, especially with a thickness of 500 μm in a typical bulk poled material [48]. Thus, the adopted poling period used to QPM in PPLT crystal is under the third-order QPM condition. The grating periods of ten waveguides used in our work provide QPM SHG for any fundamental wavelength from 793 to 805 nm at PPSLT crystal by varying temperature between 20 and 200 °C.

The 3rd QPM of PPSLT can be described as the following equation [49],

$$[n_2(\lambda_2, T) - n_1(\lambda_1, T)] = \frac{3\lambda_1}{2\Lambda(\lambda_1, T)} \tag{1}$$

where n_1 and n_2 represent the extraordinary refractive indices (n_e) of fundamental and SH waves which are related to the wavelength and temperature, λ_1 and λ_2 are the wavelength of the fundamental and SH waves, Λ is the poling period. Since a single waveguide usually corresponds to one fixed poling period, Eq. (1) can evolve to:

$$\frac{d\lambda_1}{dT} = \frac{\frac{\partial n_2}{\partial T} - \frac{\partial n_1}{\partial T}}{\frac{3}{2\Lambda} - \left(\frac{\partial n_2}{\partial \lambda_1} - \frac{\partial n_1}{\partial \lambda_1}\right)} \tag{2}$$

This equation implies that the PM wavelength versus the temperature is determined by the difference between the derivatives of the indices of the fundamental and SH waves with respect to temperature. Since the index grows with temperature more quickly under the shorter wavelength region, the numerator of right-hand side is always greater than zero for a medium with normal dispersion. The n_e of MgSLT decrease with lambda. So the derivative of n_2 with respect to λ is minus and smaller than that of n_1. As a result, the denominator of the right hand side is always positive too. Therefore, the PM lambda grows with the temperature.

Considering a fixed PM lambda, we take the derivatives of both sides of Eq. (1) and obtained:

$$\frac{d\Lambda}{dT} = -\frac{3}{2}\lambda\left[\frac{\frac{dn_2}{dT} - \frac{dn_1}{dT}}{(n_2 - n_1)^2}\right] \tag{3}$$

Since the value of the right hand side is minus, the poling period will always decreases when we elevate the PM temperature.

For a fixed temperature, the relation between the poling period and lambda can be deduced from equation that:

$$\frac{d\Lambda}{d\lambda} = \frac{3}{2}\frac{\left[(n_2 - n_1) - \lambda\left(\frac{dn_2}{d\lambda} - \frac{dn_1}{d\lambda}\right)\right]}{(n_2 - n_1)^2} \tag{4}$$

MgSLT has a normal dispersion from the violet to near infrared waveband and the refractive index decrease with the lambda. The derivative of n_2 with respect to λ is minus and smaller than that of n_1 so that the numerator of the right hand side is positive. Therefore, the poling period always grows with lambda.

Results and discussion

To illustrate the spectral tuning capability, we experientially investigate the dependence of phase-matched fundamental wavelength on the critical operating temperature at ten cladding waveguides, corresponding to different poling grating, which is illustrated in Fig. 2(b). As we can see, the phase-matched wavelength moves towards longer wavelength when the device temperature increases. Moreover, the cladding waveguides with different poling periods permit different tunable wavelength range. Fig. 2(c) depicts a series of spectra of fundamental wavelength of the waveguide No. 10 with poling period of 9.00 μm, the corresponding SHG spectra is shown in the Fig. 2(d). It is clear that the violet light is tunable from 396 to 400.8 nm by changing the laser wavelength and adjusting the PPSLT sample temperature for QPM from 60 to 200 °C, while using the fixed waveguide period. As a result, the phase-marched SH wavelength could be tuned with temperature at a tuning slope of 0.067 nm/K experimentally. Using the Sellmier equation in H. H. Lim's work [50], we obtained a temperature tuning of 0.0357 nm/K theoretically for poling period of 9 μm around fundamental wavelength of 800 nm. It is indicated that the temperature tuning of the cladding waveguides are more sensitive compared to the bulk MgSLT material, thus a more flexible PM wavelength tuning is expected. The difference between the experimental and theoretic value maybe due to the modal dispersion of the cladding waveguide structure, which is still opening for our further studies.

In order to characterize the SHG properties of waveguides in the PPMgSLT crystal, we first investigate the temperature-dependent phase-matching effects. We operate the fundamental wavelength at a fixed value of 794.4 nm, and record the second harmonic (SH) power by tuning the temperature. Fig. 3(a) illustrate the violet output power from the waveguide No. 8 with grating period of 8.96 μm as a function of the crystal temperature. It can be clearly seen that, the maximum SH power reached at 118.5 °C, replying the optimal QPM temperature. Fig. 3(b) and (c) depicts the near-filed mode profiles of SH wavelength of 397.2 nm and fundamental wavelength of 794.4 nm. Obviously, the waveguide provide a good spatial confinement at both fundamental and SH wave at a single mode manner, which is helpful for a better mode lapping and thereby opens up the possibility of a higher conversion efficiency.

We then study the dependence of the phase-matched temperature on the domain-inverted grating period by measure the temperature tuning curve of all ten of cladding waveguides with different poling periods. The ten waveguides are designed and fabricated with the grating periods ranging from 8.82 to 9.00 μm in a step of 0.02 μm. The temperature tuning curves are investigated to obtain the QPM temperature for each waveguides, which is shown in the Fig. 4(a). As can be seen, each waveguide has their own optimal QPM condition, which moves towards lower temperature when the grating period increases. For better presentation, we plot the relation between the domain periods versus phase-matched temperatures, which denoted in Fig. 4(b). There is an average shift of 7.5 °C while varying the grating period per 0.02 μm of waveguides Nos. 1–10. The experimental relation between them can also explained by the Eq. (1). Another point should be noted is that the slope of line related to the cladding waveguides shown in Fig. 4(b) is bigger than the bulks. Remembering that the cladding waveguide possess a higher temperature tuning compared to the bulk which means that difference between the two derivatives of the indices is higher for the cladding waveguide, a larger slope corresponded to the cladding waveguide in the figure is reasonable because the numerator of the right hand side of Eq. (3) also includes the same difference between the two derivatives,

We have also investigated the effect of pump wavelength on the SHG power at a fixed crystal temperature. Fig. 5(a) depicts the

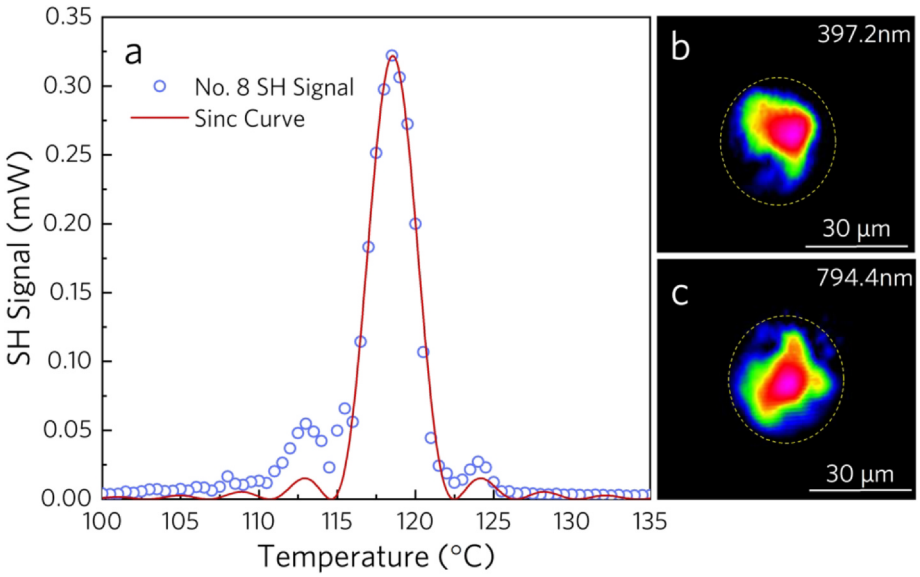

Fig. 3. (a). SH output power as a function of crystal temperature with an optimal QPM temperature of 118.5 °C at a fixed incident wavelength of 794.4 nm in waveguide No. 8 with grating period of 8.96 μm. (b) The near-field mode-profiles of second harmonic 397.2 nm and (c) fundamental wavelength 794.4 nm at the phase-matching temperature.

wavelength tuning curve by measuring the trace of SH power as a function of the fundamental wavelength at a fixed temperature of 170 °C. The measurement is also performed with the waveguide No. 8 (grating period of 8.96 μm). It can be clearly seen that there is an optimum QPM wavelength of 798.4 nm. Under this QPM wavelength, the fundamental and SH wave all demonstrate single-mode guiding, which can be seen at Fig. 5(b) and (c).

To determine the relationship of phase-matched wavelength and the period of domain inversion experimentally, we measure the wavelength tuning of all of the ten waveguides suited at different grating period in the PPMgSLT crystal, which is shown in the Fig. 6(a). Apparently, each waveguides has their own optical QPM wavelength at the fixed crystal temperature, which indicates that one can realize on-chip tunable laser source by changing the position of the fundamental wave and also achieve some multi-wavelength application. By mapping the phase-matched fundamental wavelength as a function of grating period, we obtained Fig. 6(b). As we can see, the phase-matched wavelength depends linearly on the grating period and shifts towards longer wavelength when increase the period. The fundamental wavelength change a slope of 0.7 nm while versing the grating period per 0.02 μm of waveguides Nos. 1–10. We have also plot the QPM wavelength of different periods in bulk materials. Clearly, at the same grating period, the QPM wavelength changed range is from 794.2 to 799.4 nm, which is larger than that of bulk material.

In order to determine the QPM SHG conversion efficiency of the PPMgSLT cladding waveguides, we performed measurements of the SH output power versus the guided fundamental wave power about each waveguides at their optimal QPM temperature at the fixed wavelength of 794.4 nm. The maximum SH power and corresponding conversion efficiencies of all of ten waveguides at different grating period are listed in Table. 1. The result of the ten waveguides imply the homogeneity and reproducibility of our fabrication method. One example is shown in Fig. 7, which exhibits the 397.2 nm SH power and corresponding conversion efficiency as a function of the incident 794.4 nm fundamental power. The generated violet light power varies a quadratic growth of the fundamental pump power. No fluctuation of violet beam pattern caused by photorefractive damage is observed under several hours. The normalized conversion efficiency ($W^{-1}\cdot cm^{-2}$) of the waveguides can be estimated as [11]:

$$\eta = \frac{P_{SHG}}{(P_{Pump}\cdot L)^2} = \frac{8\pi^2 d_{eff}^2}{c\varepsilon_0 n_\omega^2 n_{2\omega}\lambda_\omega^2 A_{eff}} \quad (5)$$

where P_{SHG} is the SH output power, P_{pump} is the incident fundamental wave power and L is the effective length of waveguide. d_{eff} is the effective nonlinear coefficient, for QPM doubling of order m it can be given by [51]:

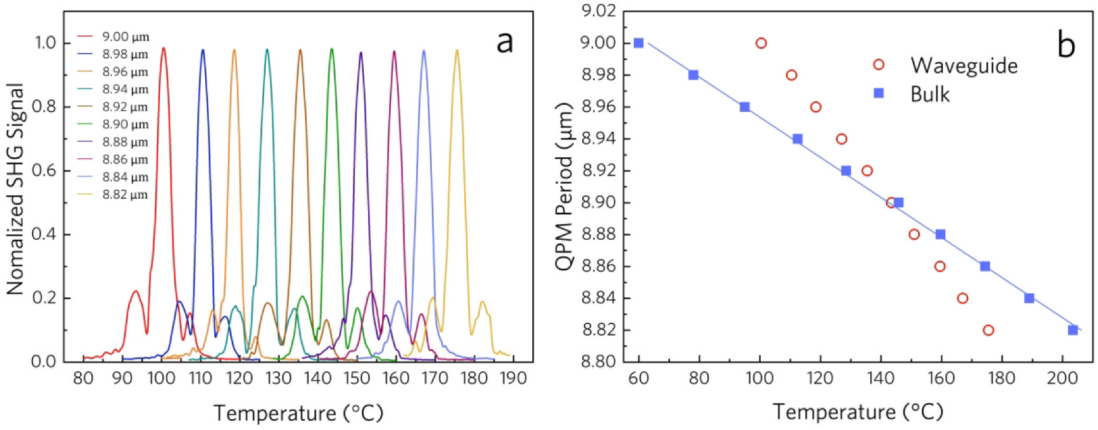

Fig. 4. (a) Normalized temperature tuning curves of all of ten waveguides with different grating periods, corresponding to different QPM temperature at a fixed incident wavelength of 794.4 nm. (b) The calculated relationship of phase-matched temperature and the period of domain inversion of bulk material. The ten circles denote the QPM temperature of ten waveguides.

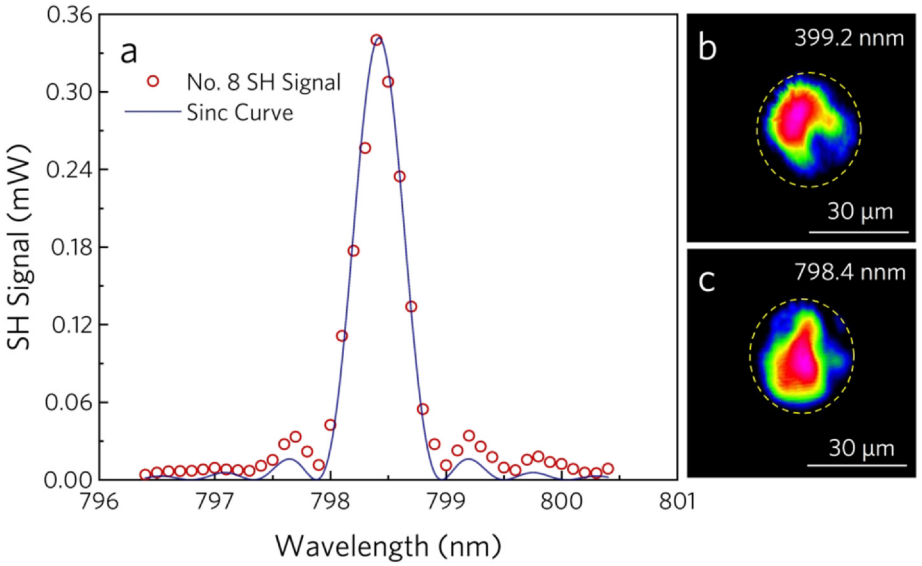

Fig. 5. Measured SH output power as a function of fundamental wavelength at a fixed temperature T = 170 °C in waveguide No. 8 with grating period of 8.96 μm. (b) The near-field mode-profiles of second harmonic 399.2 nm and (c) phase-matched fundamental wavelength 798.4 nm.

$$d_{eff} = \frac{2}{\pi m}\sin(\pi m D) d_{33} \tag{6}$$

where D is the duty cycle, as a result, the d_{eff} for third-order phase matching is 2/3π of the effective nonlinear coefficient for perfect QPM. As a result, the conversion efficiency for third-order QPM is expected a nine fold reduction compared to the first-order QPM process. The d_{eff} of MgO:PPSLT crystal is 2.85 pm/V under fundamental wavelength of 795 nm, which is comparable with the 3.2 pm/V in PPKTP crystal and large enough than the d_{eff} in BBO and LBO crystal. As can be seen in Fig. 7, a violet SH power of 0.37 mW at 397. 2 nm is generated for the fundamental input power of 336.70 mW at 794.4 nm, corresponding to the normalized conversion efficiency of 0.39%/(W·cm^2) with periodically poled length of 9.2 mm. In comparison with the third order QPM SHG at 400 nm in femtosecond laser-written waveguide of PPKTP crystal (0.02 %W^{-1}), [46] we have achieved much higher conversion efficiency. Besides the higher nonlinear performance of SLT compared to KTP crystal, we believed that the high quality of waveguide, i.e. low insertion loss, nearly undisturbed waveguide core and high overlapping between the fundamental and SH waves are also responsible for the present high conversion efficiency. In addition, this conversion efficiency is also higher than the bulk value (0.09%/W) of second-order

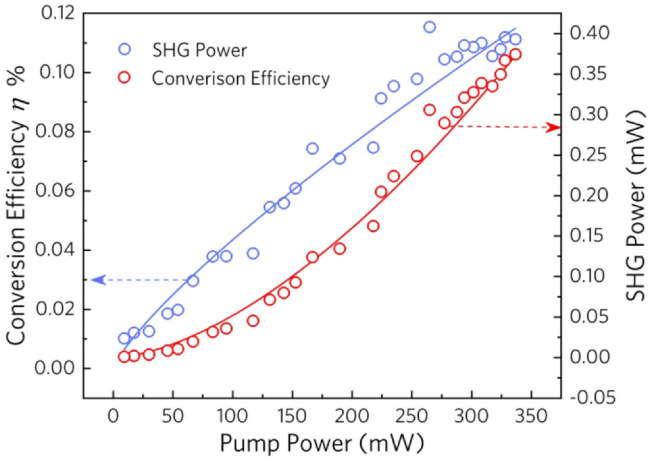

Fig. 7. Measured second harmonic output power and corresponding conversion efficiency as a function of the incident fundamental power of waveguide No. 8 at the QPM temperature of fundamental wavelength of 794.4 nm. The grating period is about 8.96 μm. The QPM temperature of PPMgSLT crystal is maintained at 118.5 °C.

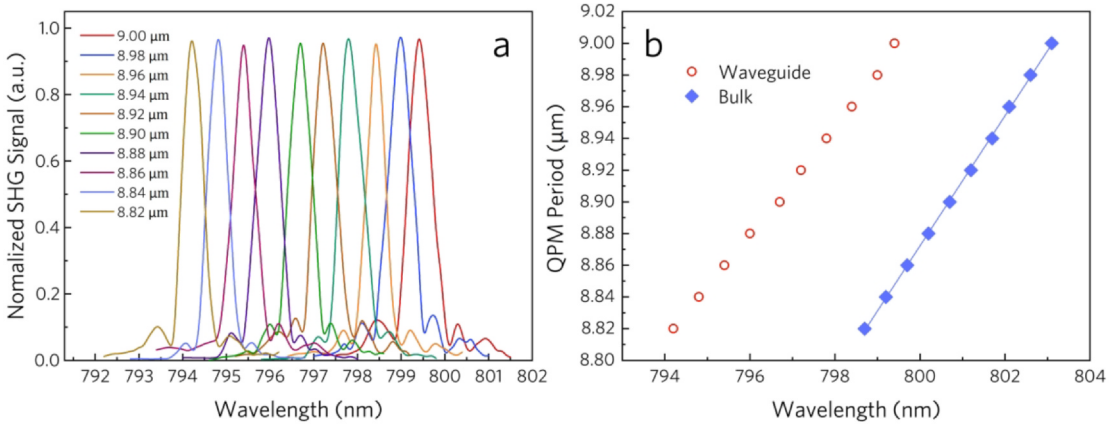

Fig. 6. Normalized wavelength tuning curves of all of ten waveguides with different grating periods, corresponding to different QPM wavelength at a fixed crystal temperature of 170 °C. (b) The calculated phase-matched wavelength as a function of period of domain inversion of bulk material. The ten circles denote the QPM wavelength of ten waveguides.

QPM SHG at 325 nm in PPLT crystal and is comparable with the value (1.2%/W) of first-order bulk QPM SHG in PPLT crystal.

Summary

In conclusion, the violet SHG has been successfully demonstrated in PPMgSLT cladding waveguides fabricated by femtosecond laser direct writing by using 3rd QPM. Ten cladding waveguides situate different positions in the fan-out domain-inverted grating pattern, corresponding to different poling periods. The insertion loss of all of ten waveguides is below 1.5 dB. Based on these waveguides and a tunable **CW** Ti:sapphire laser source, violet light of 396 to 401 nm is achieved by changing the crystal temperature. Temperature and wavelength tuning **curves** of SHG have also been investigated to find the optimal QPM condition. A comparable normalized conversion efficiency of 0.39%/(W·cm^2) is obtained at 794.4 nm fundamental wave for 8.96 μm grating period with 0.92 cm interaction length. Our results show a frequency convertor that can generate coherent violet radiation with high efficiency, opening up a potential application as on-chip light source which can be applied in the field of quantum information networks.

CRediT authorship contribution statement

LingQi Li: Visualization, Investigation, Writing - original draft. **Bin Zhang:** Visualization. **Carolina Romero:** . **Javier R. Vázquez de Aldana:** . **Lei Wang:** Conceptualization, Methodology, Software. **Feng Chen:** Supervision.

Declaration of Competing Interest

The authors declare that they have no known competing financial interests or personal relationships that could have appeared to influence the work reported in this paper.

Acknowledgements

This work was supported by the National Natural Science Foundation of China (Nos. 11874239 and 61775120); Major Program of Shandong Province Natural Science Foundation (Grant No. ZR2018ZB0649); National Key Research and Development Project (No. SQ2019YFA070063-01); MINECO (FIS2017-87970-R); and Ministerio de Economía y Competitividad de España (MAT2016-75362-C3-1-R).

References

[1] Wang W-C, Wang H-Y, Lin G-R. Sci Rep 2018;8:13142.
[2] Furch FJ, Giree A, Morales F, Anderson A, Wang Y, Schulz CP, et al. Opt Express 2016;24:19293.
[3] Riesen N, Pan X, Badek K, Ruan Y, Monro TM, Zhao J, et al. Opt Express 2018;26:12266.
[4] Wang W-C, Wang H-Y, Chen T-Y, Tsai C-T, Cheng C-H, Kuo H-C, et al. Nanophotonics 2019;8:2189.
[5] Wu L, Yan Z, Liu Y, Deng R, Jia X, Xie C, et al. Appl Phys Lett 2016;108:161102.
[6] Li L, Romero C, Vázquez JR, de Aldana L, Wang Y, Tan FC. Opt Express 2019;27:36875.
[7] Nitiss E, Yakar O, Stroganov A, Brès C-S. Opt Lett 2020;45:1958.
[8] Chen X, Karpinski P, Shvedov V, Boes A, Mitchell A, Krolikowski W, et al. Opt Lett 2016;41:2410.
[9] Hu XP, Xu P, Zhu SN. Photonics Res 2013;1:171.
[10] Yu NE, Oh M-K, Kang H, Jung C, Kim BH, Lee K-S, et al. Appl Phys Express 2014;7:012101.
[11] Wang L, Zhang X, Li L, Lu Q, Romero C, Vázquez de Aldana JR, et al. Opt Express 2019;27:2101.
[12] Lee K-S, Ko D-K, Yu NE. Jpn J Appl Phys 2017;56:040303.
[13] White RT, McKinnie IT, Butterworth SD, Baxter GW, Warrington DM, Smith PGR, et al. Appl Phys B 2003;77:547.
[14] Han Y, Wen X, Bai J, Yang B, Wang Y, He J, et al. J Opt Soc Am B 1942;2014:31.
[15] Zou X, Li W, Liang H, Liu K, Qu S, Wang QJ, et al. Opt Lett 2019;44:2791.
[16] Kianirad H, Zukauskas A, Canalias C, Laurell F. J Appl Phys 2017;121:184103.
[17] Hu P, Zhang L, Xiong J, Yin J, Zhao C, He X, et al. Opt Mater 2011;33:1677.
[18] Liu WJ, Wang HR, Tian ZS, Gao RX. Ferroelectrics Lett 2014;41:100.
[19] Aadhi A, Chaitanya NA, Jabir MV, Singh RP, Samanta GK. Opt Lett 2015;40:33.
[20] Shukla VK, Ghosh J. Phys Rev A 2020;101:023832.
[21] Hickstein DD, Kerber GC, Carlson DR, Chang L, Westly D, Srinivasan K, et al. Phys Rev Lett 2018;120:053903.
[22] Tao Y, Goh SJ, Bastiaens HMJ, van der Slot PJM, Biedron SG, Milton SV, et al. Opt Express 2017;25:3621.
[23] Kip D. Appl Phys B 1998;67:131.
[24] Ng JC, Herman PR, Qian L. Opt Lett 2017;42:195.
[25] Kores CC, Mutter P, Kianirad H, Canalias C, Laurell F. Opt Express 2018;26:33142.
[26] Wang C, Langrock C, Marandi A, Jankowski M, Zhang M, Desiatov B, et al. Optica 2018;5:1438.
[27] Oka T, Suhara T. Jpn J Appl Phys 2015;54:100304.
[28] Marangoni M, Osellame R, Ramponi R. Opt Express 2004;12:2754.
[29] Seri A, Corrielli G, Lago-Rivera D, Lenhard A, de Riedmatten H, Osellame R, et al. Optica 2018;5:934.
[30] Ródenas A, Gu M, Corrielli G, Paiè P, John S, Kar AK, et al. Nat Photonics 2019;13:105.
[31] Wei D, Wang C, Wang H, Hu X, Wei D, Fang X, et al. Nat Photonics 2018;12:596.
[32] Meany T, Gräfe M, Heilmann R, Perez-Leija A, Gross S, Steel MJ, et al. Laser Photonics Rev 2015;9:363.
[33] Sugioka K, Cheng Y. Light-Sci Appl 2014;3:149.
[34] Davis KM, Miura K, Sugimoto N, Hirao K. Opt Lett 1996;21:1729.
[35] Li L, Nie W, Li Z, Zhang B, Wang L, Haro-Gonzalez P, et al. J Lightwave Technol 2019;37:3452.
[36] Chen F, Vázquez de Aldana JR. Laser Photonics Rev 2014;8:251.
[37] Triplett M, Khaydarov J, Xu X, Marandi A, Imeshev G, Arntsen J, et al. Opt Express 2019;27:21102.
[38] Thorburn F, Lancaster A, McDaniel S, Cook G, Kar AK. Opt Express 2017;25:26166.
[39] Cheng C, Jia Y, Vázquez de Aldana JR, Tan Y, Chen F. Opt Mater 2016;51:190.
[40] Bhardwaj S, Mittholiya K, Bhatnagar A, Bernard R, Dharmadhikari JA, Mathur D, et al. Appl Optics 2017;56:5692.
[41] Imbrock J, Wesemann L, Kroesen S, Ayoub M, Denz C. Optica 2020;7:28.
[42] Nie W, Romero C, Lu Q, Vázquez de Aldana JR, Chen F. Opt Mater 2018;84:531.
[43] Muller S, Calmano T, Metz PW, Krankel C, Canalias C, Liljestrand C, et al. Opt Lett 2014;39:1274.
[44] Jia Y, Vázquez de Aldana JR, Romero C, Ren Y, Lu Q, Chen F. Appl Phys Express 2012;5:072701.
[45] Jia Y, Vázquez de Aldana JR, Lu Q, Jaque D, Chen F. Opt Mater Express 2013;3:1279.
[46] Campbell S, Thomson RR, Hand DP, Kar AK, Reid DT, Canalias C, et al. Opt Express 2007;15:17146.
[47] Almeida GFB, Martins RJ, Siqueira JP, Almeida JMP, Rodrigues Jr. JJ, Mendonça CR. Opt Mater 2018;83:229.
[48] Lu H, Wei J, Wei Y, Su J, Peng K. Opt Express 2016;24:23726.
[49] Fejer MM, Magel GA, Jundt DH, Byer RL. IEEE J Quantum Elect. 1992;28:2631.
[50] Lim HH, Kurimura S, Katagai T, Shoji I. Jpn J Appl Phys 2013;52:032601.
[51] Arie A, Rosenman G, Mahal V, Skliar A, Oron M, Katz M, et al. Opt Commun 1997;142:265.